Charles University in Prague
Faculty of Mathematics and Physics

ABSTRACT
of Doctoral Thesis

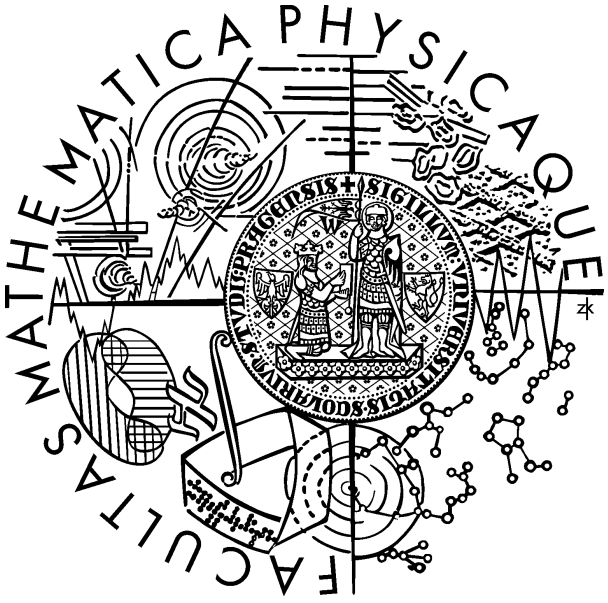

Mgr. Pavel Stránský

Classical and Quantum Chaos in Atomic Nuclei

Institute of Particle and Nuclear Physics

Supervisor: **Doc. RNDr. Pavel Cejnar, Dr.**
Branch: **F10** - Nuclear Physics

Univerzita Karlova v Praze
Matematicko-fyzikální fakulta

AUTOREFERÁT
doktorské práce

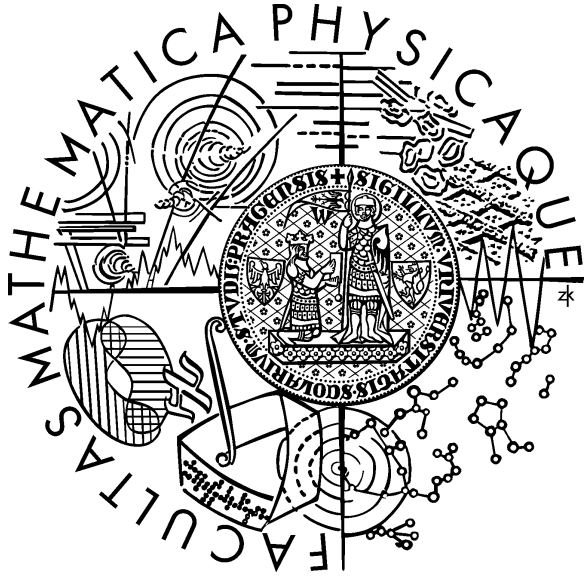

Mgr. Pavel Stránský

Klasický a kvantový chaos v atomových jádrech

Ústav částicové a jaderné fyziky

Školitel: **Doc. RNDr. Pavel Cejnar, Dr.**
Studijní program: **F10** - jaderná fyzika

Výsledky tvořící doktorskou práci byly získány během doktorského studia na Matematicko-fyzikální fakultě Unverzity Karlovy v Praze v letech 2004–2009.

Doktorand:	Mgr. Pavel Stránský Ústav částicové a jaderné fyziky V Holešovičkách 2 180 00 Praha 8
Školitel:	Doc. RNDr. Pavel Cejnar, Dr. Ústav částicové a jaderné fyziky V Holešovičkách 2 180 00 Praha 8
Školící pracoviště:	Ústav částicové a jaderné fyziky V Holešovičkách 2 180 00 Praha 8
Oponenti:	Doc. Ing. František Bečvář, DrSc. Katedra fyziky nízkých teplot V Holešovičkách 2 180 00 Praha 8
	Doc. Ing. Zdeněk Pluhař, CSc. Ústav částicové a jaderné fyziky V Holešovičkách 2 180 00 Praha 8

Tento autoreferát byl rozeslán dne: .....

Obhajoba doktorské práce se koná dne ..... v ..... hodin před Komisí pro obhajoby doktorských prací v oboru F10 – Jaderná fyzika na MFF UK, V Holešovičkách 2, Praha 8 v místnosti č. .....

S doktorskou prací je možné se seznámit na studijním oddělení děkanátu MFF UK (oddělení pro doktorské studium), Ke Karlovu 3, Praha 2.

Předseda RDSO F10:	Prof. RNDr. Jan Kvasil, DrSc. Ústav částicové a jaderné fyziky V Holešovičkách 2 180 00 Praha 8

Contents

Chapter 1

Introduction

Although models of collective dynamics of atomic nuclei [1, 2] belong to the oldest subject of nuclear physics, they still exhibit enormous potential for yielding important new results. Many of them is connected with a modern form of the collective model, the interacting boson model (IBM) [3], but purely geometric approach still provides adequate framework for the interpretation of main features of nuclear collective motions, even those accommodated within the IBM.

In the present work, we use the geometric collective model (GCM) to study the interplay between regular and chaotic behavior both in the classical and quantum case. The definition of chaos is primarily derived from the instability of classical motions, expressing the organization of trajectories in the phase space. The term "quantum chaos" [4] refers to some quantum properties—most commonly specific short- and long-range correlations in spectra of energy eigenvalues—that usually accompany the classical chaoticity. Intense study of these properties in the last decades made it possible to extend the notion of chaos from macroscopic systems to small quantum objects like atoms or nuclei.

Historically, nuclear physics offered the first confrontation of ideas related to quantum chaos with experimental data. It was when sequences of neutron resonances with a fixed spin and parity J^π were shown to agree with spectral correlations predicted by the random-matrix theory [5]. The persistence of the same kind of statistics was subsequently demonstrated [6] also for ensembles of low-energy nuclear levels (although in this case also serious deviations from chaotic correlations were detected in some families of states, particularly the collective states with $J^\pi = 2^+$ and 4^+ in even-even nuclei). Possible existence of chaotic layers of dynamics was recently discussed [7] even in connection with ground states of nuclei—in the analysis of fluctuating properties of nuclear masses.

All these data suggest that atomic nuclei at low energies exhibit a variable mixture of regular and chaotic dynamical aspects. However, very little is known about the principal mechanisms that control the competition between both types of motions. Several possible sources of irregularity can be identified already on the mean-field level, but the most substantial effects are supposed to result from residual interactions, which, however, are too difficult for explicit analysis.

A viable alternative to the attempts to solve the nuclear many-body problem in its full complexity is the use of simplified models that capture only some essential dynamical features of nuclei in various regimes [1]. Since residual interactions are responsible for highly correlated collective modes of motions (complementary to single-particle modes), one may try to search for signatures of regularity and chaos in the known elementary collective models, such as the IBM or GCM. This approach was pioneered by Alhassid *et al.* [9, 10] and by Paar *et al.* [11] using the IBM.

A detailed study of ordered and chaotic motions in the framework of the geometric collective model is presented in this work. The thesis is based particularly on published references [**I**, **II**, **VII**, **VIII**].

This abstract begins with some theoretical remarks in Chapter 2 which exposes basics of the geometric collective model and techniques of measuring chaos. We restrict ourselves to a subset of quantum levels with zero angular momentum, which makes the configuration space effectively two-dimensional, in contrast to five-dimensional space corresponding to general motions. Then we proceed to the classical version of the model (Sec. 3.1) and describe the dependence of classical measure of regularity on energy and parameters of the model and continue towards the quantum version in Sec. 3.2.

The model for zero rotations can be quantized in two physically meaningful ways. We solve the eigenvalue problem in both cases and compare the level statistics obtained, looking particularly into the regions where transitions between regular and chaotic dynamics take place. The possibility of changing the value of a classicality (Planck) constant enables us to populate the spectrum with variable density of quantum states, which is used for a global inspection of large energy domains and zooming in some finer details. By comparing the classical and quantum measures of regularity and the quantum measure calculated in various quantization schemes we test the Bohigas' conjecture [12].

We also employ the more or less forgotten graphical method invented in 1984 by Peres [13], which turns out to be very fruitful as an indicator of the changing structures across the spectrum containing possibly a very large number of states. The spectrum of stationary states of a given quantum system with two degrees of freedom is drawn as a lattice in the plane $E \times \langle P \rangle$, where E is energy and $\langle P \rangle$ stands for an arbitrary observable average. This allows one to recognize ordered and disordered patterns and visually allocate regular and chaotic domains within the same energy interval. Finally, the abstract is closed by the conclusion.

Chapter 2

Theoretical outline

2.1 Geometric collective model

2.1.1 Hamiltonian

We consider the Hamiltonian of the geometric collective model (GCM) [14] in the truncated form

$$\begin{aligned} H =& \frac{\sqrt{5}}{2K}\left[\boldsymbol{\pi}\times\boldsymbol{\pi}\right]^{(0)} + \\ &+\sqrt{5}\,A\left[\boldsymbol{\alpha}\times\boldsymbol{\alpha}\right]^{(0)} - \sqrt{\frac{35}{2}}\,B\left[\left[\boldsymbol{\alpha}\times\boldsymbol{\alpha}\right]^{(2)}\times\boldsymbol{\alpha}\right]^{(0)} + 5\,C\left(\left[\boldsymbol{\alpha}\times\boldsymbol{\alpha}\right]^{(0)}\right)^2 \end{aligned} \tag{1}$$

where α_μ, $\mu = -2,\ldots,2$ form the spherical tensor of quadrupole shape variables (they can be viewed as coefficients at the $Y_{2\mu}$ spherical harmonics in an expansion of nuclear radius), having five independent real components, $\pi_\mu = -K(\mathrm{d}\alpha^*_\mu/\mathrm{d}t)$ the associated tensor of momenta, and $[\bullet\times\bullet]^{(\lambda)}$ stands for the coupling to angular momentum λ. The constants $\{K, A, B, C\}$ are adjustable parameters. We neglect higher-order terms of the Hamiltonian, in particular the 3rd-order kinetic term.

The transformation into the principal frame of deformation yields the potential in the form

$$\begin{aligned} V &= A\beta^2 + B\beta^3\cos 3\gamma + C\beta^4 = \\ &= A\left(x^2+y^2\right) + B\left(x^3 - 3xy^2\right) + C\left(x^2+y^2\right)^2, \end{aligned} \tag{2}$$

where we use the usual parametrization [1]:

$$\begin{aligned} \alpha_0 &\equiv x = \beta\cos\gamma \\ \sqrt{2}\,\alpha_2 &\equiv y = \beta\sin\gamma. \end{aligned} \tag{3}$$

The system described by Eq. (1) has five degrees of freedom. The tensor $\boldsymbol{\alpha}$ can be diagonalized to get two shape coordinates x and y (or β and γ) and three Euler angles $\{\theta_1, \theta_2, \theta_3\}$ characterizing the relative orientation of the principal and laboratory frames.

Parameters β and γ represent the known Bohr variables; $\beta = 0$ stands for spherical shape, $\beta > 0$ implies nonzero deformation with prolate or oblate axially deformed shape for γ equal to even or odd multiples of $\pi/3$, respectively.

We restrict ourselves to the the nonrotating case $\boldsymbol{J} = 0$: the principal frame is at rest and the motion can be described solely in terms of x and y (or equivalently in terms of β and γ). In this case our system is effectively two dimensional (2D).

It is worth mentioning that the system is integrable for $B = 0$ and the parameter B governs the strength of nonintegrable perturbation. We denote the nonintegrable term of the potential (2) as

$$H' = \beta^3 \cos 3\gamma. \tag{4}$$

2.1.2 Scaling properties and phase diagram

Hamiltonian (1) contains four external parameters. Without the loss of generality, the fundamental physical units of the system can be chosen such that three out of the four parameters become equal to unity or to ± 1 for A, while the remaining parameter takes the role of the external variable. The only fundamental parameter, determining the type of equilibrium shape of the nuclei, can be introduced as

$$\tau \equiv \frac{AC}{B^2}. \tag{5}$$

In the quantum case, the classicality parameter

$$\kappa \equiv \frac{\hbar^2}{K}, \tag{6}$$

whose changes can be viewed either as changes of the Planck constant, or as changes of the mass, constitutes the second independent parameter of the model. This parameter determines the absolute density of states.

In the whole work we fix $C = 1$ and $K = 1$.

Figure 1 shows the phase structure of the geometric model. Gray parabolae $\tau =$ const. (or paraboloids, if the third coordinate of the parametric space corresponding to the parameter C is considered) represent sets of parameters giving scale-equivalent Hamiltonians. Thick solid lines $A < 0$, $B = 0$ and $\tau = 1/4$ depict first-order phase transitions between prolate and oblate shape and between deformed and spherical shape, respectively. Dotted line, which can be expressed explicitly as

$$\begin{aligned} &A = -1, B \in (0, 1) \\ &A \in (-1, 1), B = 1 \\ &A = 1, B \in (1, 0), \end{aligned} \tag{7}$$

represents the curve which crosses all parabolae. It is profitable to present the results on this path.

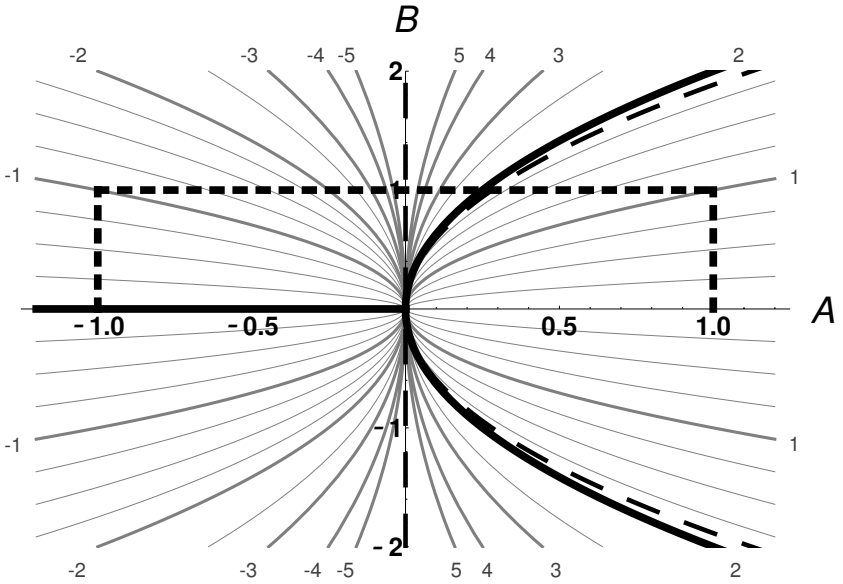

Figure 1: The GCM phase diagram in the plane of parameters A and B for any $C > 0$. Thick solid lines represent phase separatrices (first-order), thick dashed lines enclose the region of phase coexistence. Thin gray parabolae correspond to dynamically equivalent parameter sets related by scaling transformations. They are marked with values $\pm 1/\sqrt{|\tau|}$. Dotted line depicts the path which passes through all different configurations of the GCM system.

2.1.3 Quantization and diagonalization

Standard quantization procedure with $\pi_\mu = -i\hbar\frac{\partial}{\partial\alpha_\mu}$ (satisfying comutation relation $[\alpha_\mu, \pi_\nu] = i\hbar\delta_{\mu\nu}$) leads to the kinetic term [1]

$$T^{(5\mathrm{D})} = -\frac{\hbar^2}{2K}\left(\frac{1}{\beta^4}\frac{\partial}{\partial\beta}\beta^4\frac{\partial}{\partial\beta} + \frac{1}{\beta^2\sin 3\gamma}\frac{\partial}{\partial\gamma}\sin 3\gamma\frac{\partial}{\partial\gamma}\right) + T_{\mathrm{rot}}, \tag{8}$$

where T_{rot} stands for a nontrivial rotational part of the kinetic energy, containing the derivatives with respect to Euler angles and coupling all five dynamical variables (this is the reason for the notation 5D). However, in the considered nonrotating case this term is identically zero, $T_{\mathrm{rot}} = 0$, and only the two vibrational degrees of freedom remain.

For $\boldsymbol{J} = 0$ the truly 2D scheme represents an alternative way of quantization. It means that we put the system into the intrinsic frame first and only then carry out the quantization. The kinetic term obtained in this way reads as follows:

$$T^{(2\mathrm{D})} = -\frac{\hbar^2}{2K}\left(\frac{1}{\beta}\frac{\partial}{\partial\beta}\beta\frac{\partial}{\partial\beta} + \frac{1}{\beta^2}\frac{\partial^2}{\partial\gamma^2}\right), \tag{9}$$

which is nothing but the standard 2D kinetic energy expressed in polar coordinates $(r, \phi) \equiv (\beta, \gamma)$.

We diagonalize both types of the GCM Hamiltonian in the respective 2D or 5D harmonic oscillator bases. While the original 5D solution possesses several implicit symmetries arising from the ambiguity of the system's orientation in the intrinsic frame, solutions of the 2D model do not a priori satisfy such symmetries. If the spectra and

spectral statistics associated with both quantizations are to be compared, conditions of symmetries need to be imposed externally also to the 2D case. In addition, if we slightly relax the conditions, we can split the 2D quantization scheme into the odd and even cases, which gives us another independent class of 2D solutions.

Both expressions (8) and (9) have the same classical limit and offer a possibility to study the influence of the quantization method on the quantum chaotic features of the spectrum. Let us stress that in the nuclear physics context only the 5D quantization is correct.

2.2 Measuring and visualising chaos

2.2.1 Fraction of regularity

At first we introduce the measure of classical regularity. Trajectories in the phase space of an integrable system with 2 degrees of freedom lie on surfaces that are topologically equivalent to 4D tori. In crossings with a plane (the so called *Poincaré section*) such tori form sets of 1D curves (ovals) which are covered by passages of individual trajectories (periodic orbits create just sequences of isolated points on these curves). On the contrary, a fully chaotic system is subject to the ergodic principle which ensures that orbits uniformly cover the whole kinematically accessible area of the Poincaré section. In intermediate cases—for partially chaotic/regular systems—the randomly covered areas in the Poincaré section coexist with regular islands, remnants of tori. An example of a Poincaré section is shown in Fig. 2.

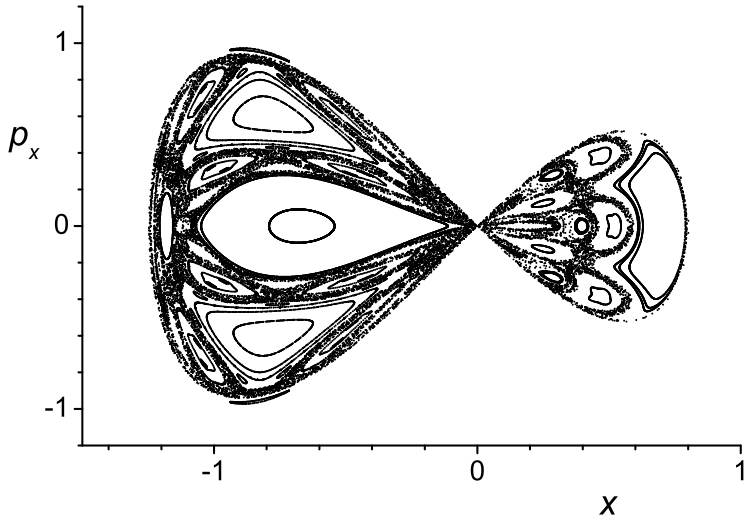

Figure 2: An example of the Poincaré section. Each dot corresponds to the passage of one trajectory of the GCM system with parameters $A = -1$, $B = 0.446$, and energy $E = 0$ through the plane $y = 0$ (in this figure we show altogether 50000 such crossings of 52 randomly chosen trajectories).

We quantify the degree of regularity in case of $\mathbf{J} = 0$ by a relative fraction of regular islands in the Poincaré section. More specifically, we introduce the ratio

$$f_{\mathrm{reg}} = \frac{S_{\mathrm{reg}}}{S_{\mathrm{tot}}}\,, \tag{10}$$

where S_{reg} is the area corresponding to all regular islands in the $y = 0$ Poincaré section and S_{tot} is the total kinematically accessible area of the same section. Fraction (10) may change between limiting values 0 (complete chaos) and 1 (perfect order) as the external control parameter A and energy E vary.

Regular fraction f_{reg} would be determined through dividing the total area of the section into an infinite grid of cells and labeling each cell according to whether it is crossed by a regular or chaotic trajectory, which are distinguished by the Smaller alignment indices method (SALI) [15]. More details concerning the calculation of f_{reg} are given in articles [**I**, **II**, **V**].

2.2.2 Spectral statistics

In this subsection we turn to measuring quantum chaos. According to Bohigas' conjecture [12], chaotic systems exhibit strong correlations between levels, which result in an effect known as "spectral rigidity". The short-range component of these correlations is most clearly manifested in the distribution of the nearest-neighbor spacings (NNS), i.e. gaps between neighboring levels in a transformed (so-called unfolded) spectrum. In fully chaotic systems, this distribution is amazingly well approximated by the Wigner distribution, while in systems with regular classical counterparts the NNS distribution tends to be Poissonian.

A suitable quantity allowing one to interpolate between the two limiting cases is the Brody parameter ω [16]. It is defined through the distribution

$$\begin{aligned} P_{\mathrm{B}}(s;\omega) &= (\omega+1)\mathcal{N}_\omega\, s^\omega \exp\left(-\mathcal{N}_\omega\, s^{\omega+1}\right) \\ \mathcal{N}_\omega &= \left[\Gamma\left(\frac{\omega+2}{\omega+1}\right)\right]^{\omega+1}, \end{aligned} \tag{11}$$

where s is the spacing between adjacent levels in the unfolded spectrum and $\mathcal{N}_\omega$ a factor resulting from the required conditions $\int_0^\infty P_{\mathrm{B}}(s;\omega)ds = 1$ (normalization) and $\int_0^\infty sP_{\mathrm{B}}(s;\omega)ds = 1$ (unfolding). Eq. (11) interpolates between the Poisson ($\omega = 0$) and Wigner ($\omega = 1$) distributions, hence a value $\omega \in \langle 0, 1\rangle$ obtained from a concrete spectrum tells us where between order and chaos the actual system is. The adjunct $(1-\omega)$ of the Brody parameter can be directly compared with the regular fraction f_{reg}.

Practically we proceed as follows: We divide the calculated spectra (usually we are able to find 30000 well-converging levels) into windows of 1000 levels and after unfolding procedure we estimate the Brody parameter for each window via the χ^2 fit, applied to the cumulative distribution function

$$R_{\mathrm{B}}(s;\omega) \equiv \int_0^s P_{\mathrm{B}}(s';\omega)\mathrm{d}s' = 1 - \mathrm{e}^{-\mathcal{N}_\omega\, s^{\omega+1}}. \tag{12}$$

As a result of this procedure we obtain energetical dependence of the Brody parameter.

2.2.3 Peres method

Quantum measures of chaos are usually based on certain statistical properties of the spectra of energy levels, e.g. on the nearest-neighbor-spacing distribution (and the related Brody parameter ω, see previous section) or on the long range correlations of eigenvalues [17]. It is clear that the statistics describes only some bulk features of a sufficiently large portion of the spectrum. However, the method introduced by Peres in 1984 [13] makes it possible to assign regular, chaotic, or a mixed type of dynamics to *individual states*. Peres' method is entirely visual and can be considered as a quantum analogue of the classical technique based on the Poincaré sections.

The method can be briefly described as follows: Having an arbitrary constant of motion A in an integrable conservative system and drawing its eigenvalues A_i against energies E_i of individual levels i, the resulting image forms a fully regular lattice (due to the EBK quantization). Since the constant of motion A can be unknown or even does not exist (in nonintegrable systems), Peres proposed to take the time average of an arbitrary observable P. The operator corresponding to this average commutes with the Hamiltonian, or its classical Poisson brackets vanishes. In practice it means that we calculate expectation values $\langle P \rangle_i$ for individual eigenstates and plot them against E_i. It can be shown that in an integrable (regular) system such a lattice is formed by ordered patterns, while chaotic (or mixed) systems exhibit (partly) disordered lattices.

In the geometric model we consider two different Peres operators. The first one is identified with the square of the angular momentum operator L connected with the rotations varying angle γ. In the 2D case, this is the Casimir invariant of the O(2) algebra of rotations in the (β, γ) plane:

$$L^2_{\mathrm{2D}} = \hbar^2 \frac{\partial^2}{\partial \gamma^2}. \tag{13}$$

In the 5D case, L^2 is the Casimir invariant of the GCM algebra O(5) [18] restricted to value $\boldsymbol{J} = 0$ of the O(3) angular momentum (null rotations in the ordinary space). We have

$$L^2_{\mathrm{5D}} = \frac{\hbar^2}{\sin 3\gamma} \frac{\partial}{\partial \gamma} \sin 3\gamma \frac{\partial}{\partial \gamma}. \tag{14}$$

The second Peres operator used in our analysis correspond to the nonintegrable perturbation H' of the Hamiltonian, given by Eq. (4).

Chapter 3

Numerical results

3.1 Classical Chaos in the GCM

The fraction of regularity $f_{\rm reg}$ for given parameter and energy is calculated by means of the method described in Sec. 2.2.1. The complete map of $f_{\rm reg}$ in the nonrotating case of the GCM system (1) is depicted in Fig. 3. The horizontal axis shows the values of a free parameter of the system and is divided by thick white lines into three regions with different scalings, following the path expressed by Eq. (7). The vertical axis shows the energy. The regularity with extremely interesting behavior at absolute energy $E = 0$, which corresponds for $A < 0$ to a local maximum of the potential (2) at $\beta = 0$, is presented separately in Fig. 4.

Both leftmost and rightmost parts of the figure correspond to the integrable case $B = 0$ with $f_{\rm reg} = 1$. As no explicit second integral of motions is known for $B \neq 0$, we expect increasing chaos when the integrable limit $B = 0$ is being departed. This is, however, not quite so. The dependence of $f_{\rm reg}$ on energy and a control parameter of the system exhibits very complex nonmonotonous behavior, involving virtually integrable regions. The most important well-pronounced island of regularity in a wide range of energies is observed at $B \approx 0.6$. As shown in Ref. [**III**], this region is connected with the so-called regular arc of the interacting boson model [9, 10]. Increased values of the regular fraction are also observed for other values of the adjustable parameter at $E \approx 0$, see Fig. 4.

The degree of chaos also depends on energy. For E close to the minimal value of the potential (2), the system performs nearly harmonic vibrations around one of the minima. For $E \gg 0$, one again expects regular behavior as the quartic term in potential (2) completely prevails (see Refs. [**I**, **II**]). In the intermediate region of energies, striking areas with high regularity is observed. The bands of full regularity—the strong one clearly visible at energy $E \approx 24$ for $A \gtrapprox -1.2$ in the scaling $B = 1$ and followed by a smaller one at $E \approx 7$ for $A \gtrapprox 0.6$ in the same scaling—still remain unexplained.

Dash black line in the Fig. 3 encircles the area where the kinematically accessible region have concave border. In the geometric model, the lower part of the line (up to energies $E \approx 1$) corresponds exactly with the curve obtained by the method using Riemannian geometry [19], which should separate regions with regular and chaotic dy-

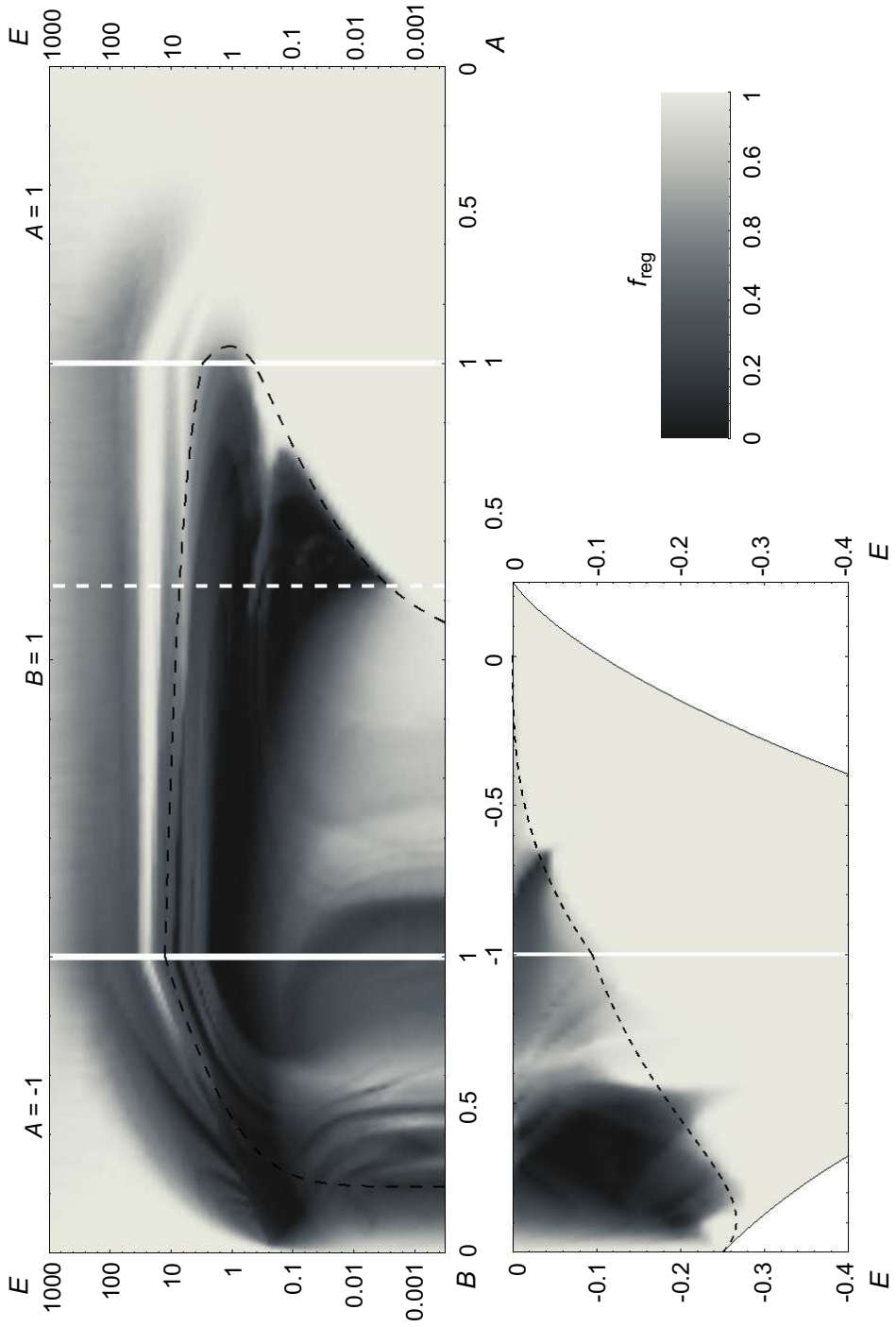

Figure 3: Complete map of classical regular fraction f_{reg} as a function of control parameters and energy E. The degree of chaos is coded in shades of gray, with light gray (black) corresponding to complete order (chaos). The plot is divided by the thick white lines into three regions with different scaling ($A = -1$, $B = 1$, and $A = 1$, respectively), according to the path expressed by Eq. (7). White dashed line indicates the deformed-spherical shape phase transition. Black dashed line corresponds to the convex-concave transition of the border of kinematically accessible area (concave shape is confined inside). The absolute error of the calculation of f_{reg} does not exceed 0.02.

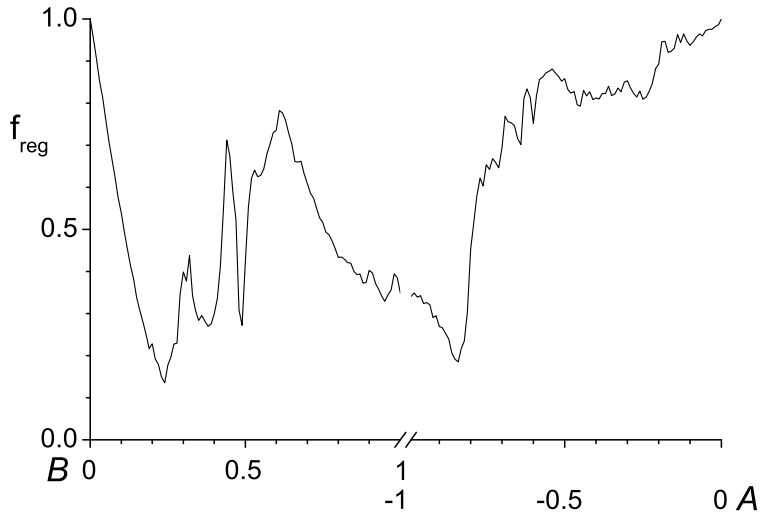

Figure 4: The regular fraction $f_{\rm reg}$ for $E = 0$ as a function of B (scaling $A = -1$, the left part of the graph) and of A (scaling $B = 1$, the right part of the graph).

namics. However, it is evident from the figure that this geometrical criterion gives only approximate estimation of the place where regularity falls into chaos. Generally one observes that chaotic regions slightly penetrate out through the separation line with some exceptions appearing, e.g., near the arc of regularity $B \approx 0.6$.

3.2 Quantum chaos in the GCM

3.2.1 Brody parameter

We compare the quantum measure of regularity (Brody parameter), obtained in the way described in Sec. 2.2.2, with the corresponding classical measure $f_{\rm reg}$ from Fig. 3.

Figure 5 depicts the dependence of both measures $f_{\rm reg}$ and $(1 - \omega)$ on energy. The value of the Hamiltonian parameter B was chosen as $B = 1.09$ The energy range shown in the figures represents the most interesting region, lying between the domains of full regularity at very low and very high energies. As was mentioned above, for energies just above the global minimum of the potential the system is entirely regular due to the validity of the harmonic-well approximation. With increasing energy, the regularity suddenly breaks down and continues falling sharply until it nearly reaches zero. After this stage, it takes off again and exhibits several well pronounced peaks of highly regular motions, which are separated by valleys of more chaotic dynamics. For sufficiently high energies, not shown in the present figure, the regularity starts growing steadily toward the fully regular limit, following roughly a logarithmic dependence.

Classical measure $f_{\rm reg}$, taken from the vertical section of the Fig. 3 at $B = 0.62$, is drawn by the solid line, the energy dependence of the adjunct of the Brody parameter

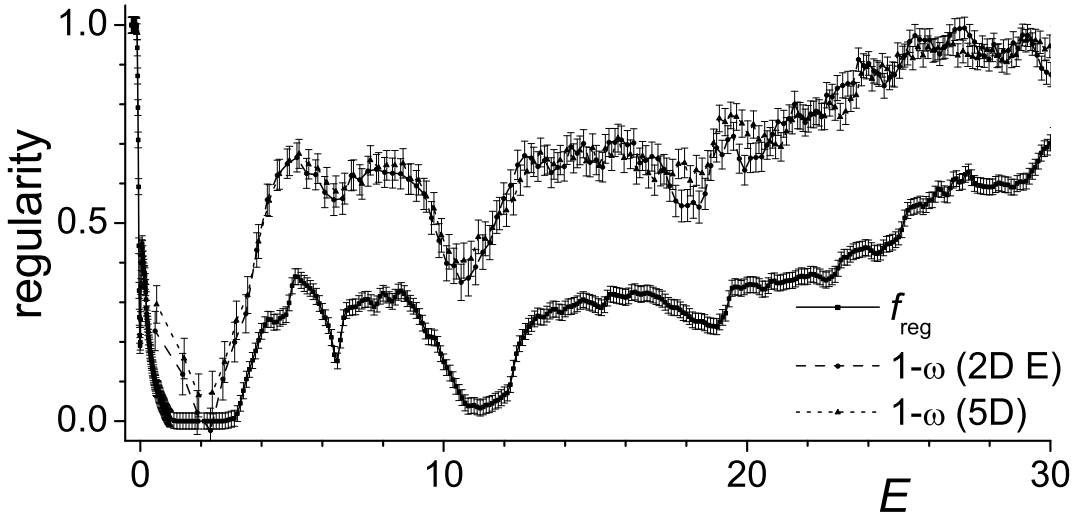

Figure 5: A comparison between the classical regular fraction $f_{\rm reg}$ and an adjunct $(1-\omega)$ of the Brody parameter for $B = 1.09$ calculated in two different types of quantization (dash line correspond to the 2D even case, dotted line to the 5D case).

$(1-\omega)$ by the dashed and dotted line for 2D even and 5D quantization scheme, respectively. Observed maxima and minima of all curves coincide, however, it turns out that the Brody parameter tends to slightly overestimate the regularity. Indeed, there is no reason to expect that $f_{\rm reg}$ and $(1-\omega)$ behave in exactly the same way. We only expect a qualitative agreement, and that is fully confirmed in the present calculation.

In this figure we can also observe the dependence of the quantum measure of chaos on the method of quantization. Although the spectra obtained by various types of quantizations differ from each other distinctly, the Brody parameter for all quantization schemes exhibits essentially the same dependence on energy, the mutual deviations being fully within the range of standard errors. Therefore, we can report that full agreement with Bohigas' conjecture is confirmed in the present model independently of the chosen quantization scheme.

More detailed discussion concerning the correspondence of classical and quantum measures of chaos of is presented in the article [**VII**].

3.2.2 Peres lattices

We construct the Peres lattices in the GCM system for two independent operators L^2 and H', see Sec. 2.2.3.

First of all, we show the decay of regularity with increasing perturbation B, depicted in Fig. 6. Panel (a) demonstrates the fully regular lattices for the integrable case $B = 0$ (the average value $\langle H' \rangle$ is identically zero in this case). It is worth emphasizing that the lattice in an integrable case is regular for *any* averaged operator. As can be seen in panel

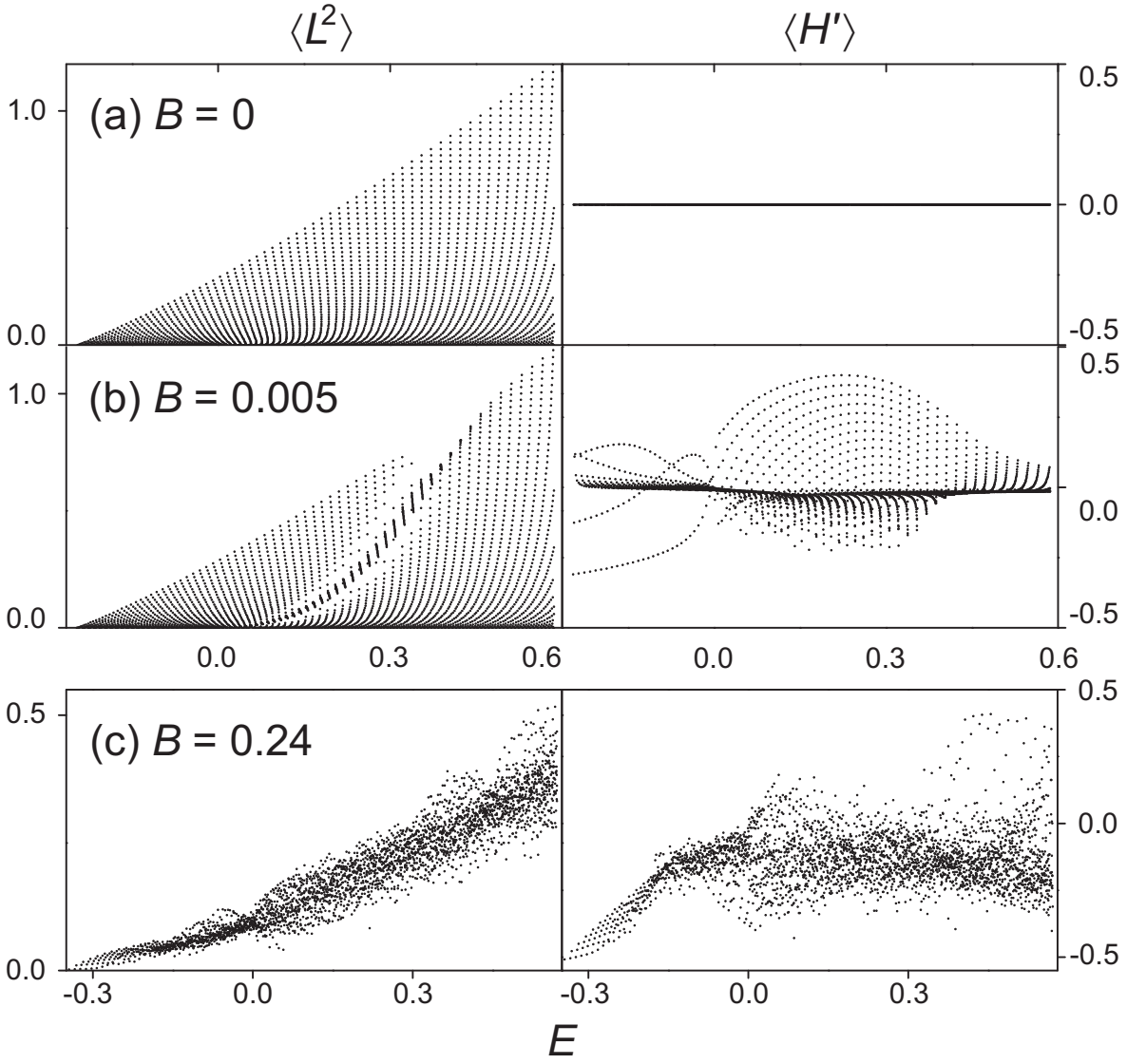

Figure 6: Peres lattices for $\boldsymbol{J} = 0$ eigenstates of the GCM in the 2D even quantization ($\hbar = 0.005$) with 3000 levels plotted. The points represent individual eigenstates with coordinates E_i (energy) and $\langle P \rangle_i$ (expectation value of the respective Peres operator). Two Peres operators, L^2 (left column) and H' (right column) are taken into account. Row (a) correspond to the fully integrable case, $B = 0$. Row (b) depicts the disturbance of the lattice with small nonintegrable perturbation, $B = 0.05$. Row (c) shows the most chaotic case, $B = 0.24$.

(b), adding a small perturbation to the integrable Hamiltonian does not instantaneously break down the entire regular lattice. Instead, some localized seeds of distortion are created, while the rest of the lattice remains ordered in the same fashion as in the integrable case. This scenario is in accordance with Percival's conjecture [20] assuming that the sets of regular and chaotic eigenstates are statistically independent in the semiclassical limit $\hbar \to 0$, i.e. they do not interact with each other. Therefore, the persisting regular parts of the lattice can be associated with surviving remnants of classical tori, while the disordered parts correspond to proliferating chaotic orbits. As the perturbation strength B grows, the remnants of tori are gradually disappearing and disorder tends to increasingly plague the lattice. This is demonstrated by an almost totally disordered lattice in panel (c), where only a few low lying states keeps the regular pattern.

The above-outlined visual method allows one to judge which parts of a mixed spectrum (or, in optimal cases, which individual states) are regular and which are chaotic, in contrast to traditional methods of quantum chaos based on the spectral statistics. since in that case regular and chaotic (or mixed) parts of the spectrum can only be specified by energy. In the present approach, these parts can coexist within the same energy interval, the additional information needed for their separation being obtained from the behavior of the averages $\langle P \rangle_i$.

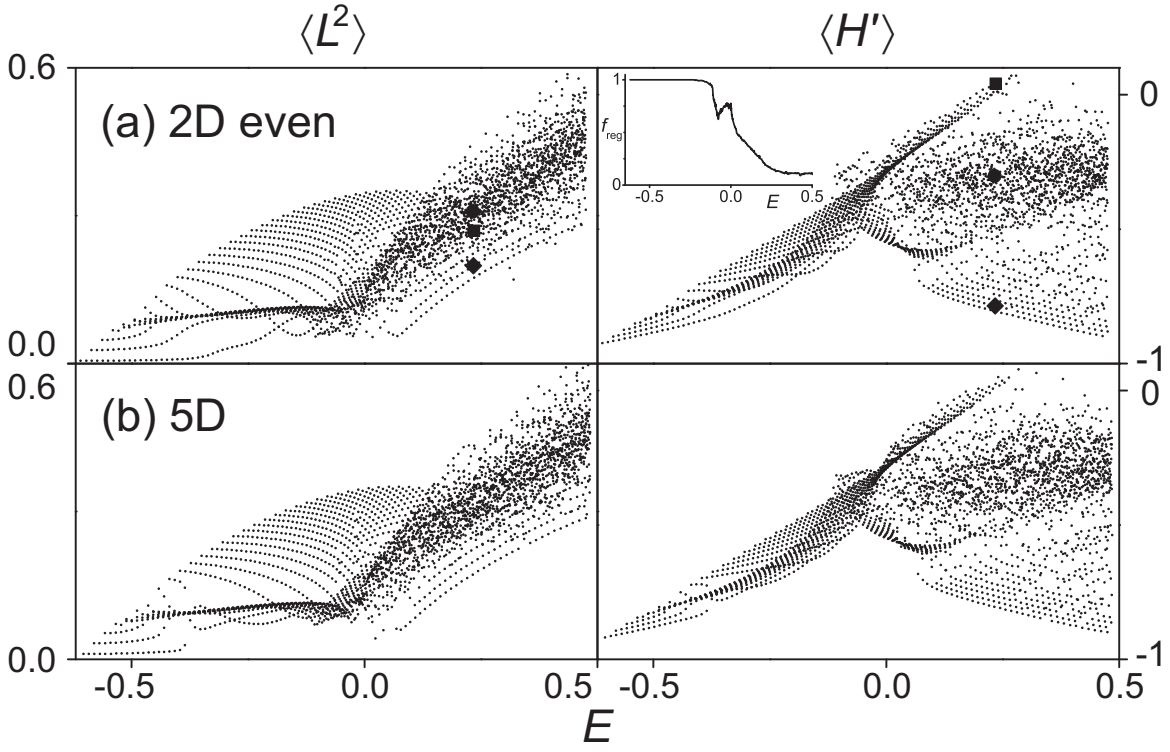

Figure 7: Peres lattices of the GCM at $A = -1$, $B = 0.62$ with averages of L^2 (left) and H' (right) for 2D even (row a) and 5D (row b) quantizations ($\hbar = 0.005$). In row (a), three states denoted by full symbols are identified in both lattices. In the inset of the top right panel the energetical dependence of the classical regular fraction $f_{\rm reg}$ is shown.

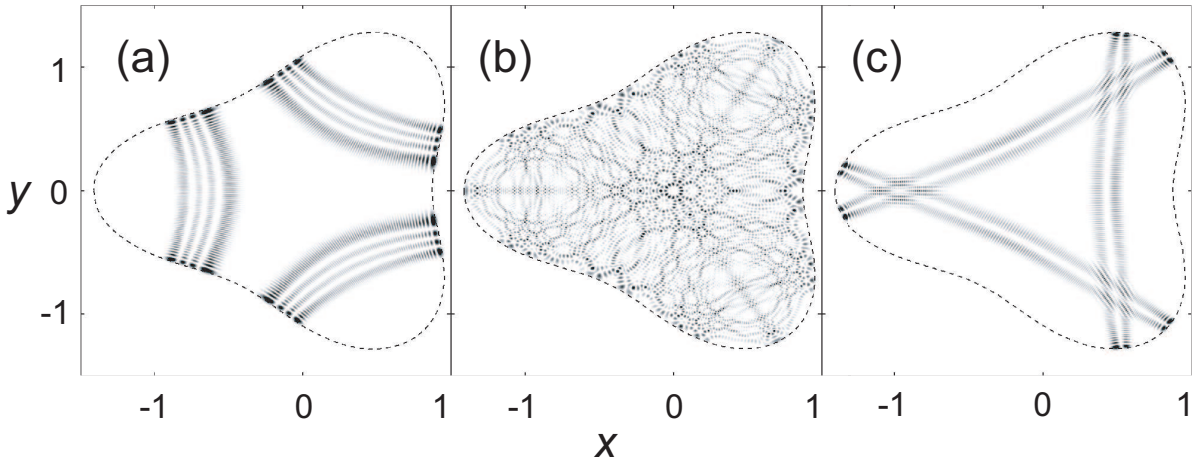

Figure 8: Squared wave functions for the three marked states from Fig. 7 (2D even quantization). The states (a) and (c), which correspond to the square and the diamond, respectively, are taken from the regular part of the lattice (the 1995th and 1885th level, respectively). The state (b), associated with the bullet, belongs to the chaotic part (the 1890th level), showing an ergodic behavior.

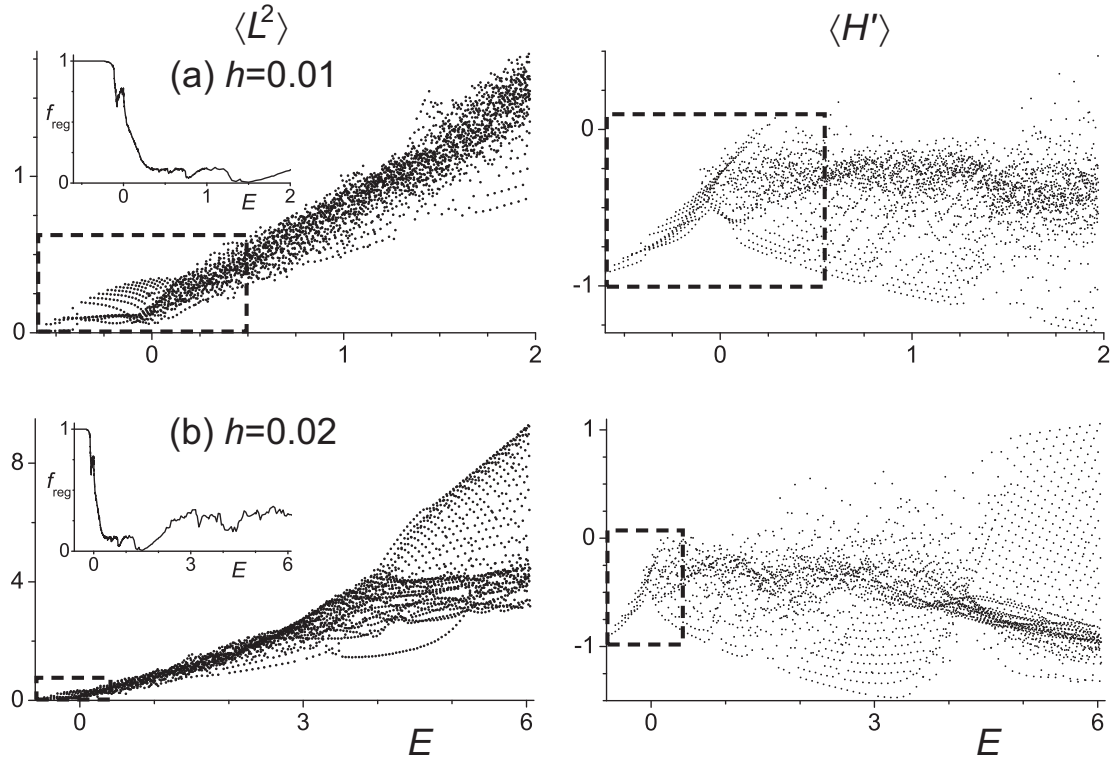

Figure 9: The same as in Fig. 7, but only for 2D even quantizations and different values of Planck constant: $\hbar = 0.01$ (row a) and $\hbar = 0.02$ (row b). Dashed boxes enclose the same area of each column as is shown in Fig. 7.

In Fig. 7 we compare Peres lattices obtained (for both Peres operators) in the 2D even and 5D quantizations. The value $B = 0.62$ belongs to the island of strongly pronounced regularity close to the resonance of β and γ vibrations, see Sec. 3.1. The regularity shows up as a large area of ordered points, which starts at the lowest negative energies and spreads over to positive energies, where it is joined by a rising chaotic area. Despite the spectra for different quantizations show significant differences, the form of Peres lattices is rather similar.

In order to demonstrate the coincidence of the regular and chaotic regions in the lattices for different Peres operators, we have highlighted three of the states in the first row of Fig. 7, marking them by a square, a bullet, and a diamond. Probability densities for the corresponding wave functions are depicted in Fig. 8. The wave functions as well as the location of the respective points in the Peres lattice show that the square and the diamond correspond to regular states, while the bullet represents a chaotic state. In Fig. 7(a) we see that this assignment is consistent for both choices of the Peres operator. Let us note that both regular levels (a) and (c) in Fig. 8 exhibit a large increase of the wave-function magnitude in a region where a certain periodic trajectory oscillates in the classical case [4].

Although we can choose an arbitrary operator for plotting the Peres lattice, Fig. 7 indicates that some operators may be more suitable than others. For some choices, a part of the regular region in the lattice can pervade into the chaotic area and hide there behind a disordered mesh of points. In such cases, one cannot decide whether a level inside a chaotic region is indeed chaotic. (On the other hand, overlapping regular areas form a regular area again.) While there is no doubt that these observations demonstrate limitations of the Peres method, one can improve its resolution by employing several incompatible Peres operators. Indeed, Fig. 7 (right) shows that for the three highlighted states a better choice of Peres operator is $P = H'$.

Figure 9 displays Peres lattices for 2D even quantization with different Planck constant $\hbar$. Tuning the value of $\hbar$—which is proportional to the classicality constant κ, see Eq. 6—one scales the absolute density of quantum states. Here we want to show that these changes do not influence the main features of the Peres lattice. The variations of the lattice with $\hbar = 0.005, 0.01, 0.02$ for both Peres operators are observed in Figs. 7 and 9. The structures with well pronounced minima and maxima of the dependence classical regular fraction f_{reg} on energy is shown in the insets. A decrease of the $\hbar$ value increases the density of states (the system gets closer to the classical limit) and serves as a zoom into the sea of levels: one can see finer details of the lattice but (because of computational limits) a smaller fraction of the spectrum is available. For a comparison, the thick dashed box in both panels of the same column of Fig. 9 encloses a fixed region of energy $\times$ P-average from Fig. 7. It is seen that the structures observed in the lattice become wealthier in details as κ decreases, but the overall appearance of the relevant part of the lattice remains the same.

Peres lattices in the geometric collective model are fully discussed in Ref. [**VIII**].

Chapter 4

Conclusion

In this work we studied $\boldsymbol{J} = 0$ vibrations in the geometric collective model, that captures the most essential collective degrees of freedom in nuclei. In spite of the model's conceptual simplicity, it exhibits enormous complexity of solutions, with a very sensitive dependence of the observed behaviors on external parameters and energy. These features qualify the model for being a subject of detailed analyses of the competition between regular and chaotic modes of motions on both classical and quantum levels.

First we have analyzed classical chaos which allowed us to to understand the classical character of various types of motions that emerge in different regimes of nuclear collective dynamics, in particular those involved in the competition between regular and chaotic features. We have demonstrated that the GCM exhibits an unexpectedly complex interplay between regular and chaotic types of motions. The important result is the discovery of two well-pronounced quasiregular islands in intermediate domains of the control parameter B and energy E. One of these islands resides at low energies, $E < 1$, in the range approximately $B \approx 0.6$, $A = -1$, and the other one at intermediate energies, $E \approx 24$, within the interval $A \in (-1.2, \infty)$, see Fig. 3. While the latter quasiregular region is probably too high in excitation energy to be relevant experimentally, the former one is undoubtedly a close relative of the IBM "arc of regularity" [9, 10]. It needs to be stressed that the origin of regularity in the above domains still remains rather unclear. On the other hand, the mechanism underlying the emergence of chaos in nuclear collective motions at the lowest energies was identified with the convex–concave transition of the shape of the kinematically accessible area in the plane of deformation parameters, which exactly correspond to the regular-chaos transition obtained by the geometric method [19].

The framework of quantized geometric model allowed us to study the correspondence between classical and quantum measures of chaos. Although the dependence of chaotic measures on some external control parameters has been extensively studied in quantum billiards, see e.g. Refs. [21, 22], the dependence on energy has been marginalized so far. This is partly because billiard systems do not permit this kind of analysis—their chaotic features are always uniform in energy. Even the studies based on "soft" potential systems have been so far focused mostly on the cases with a relatively simple energy dependence of chaotic measures, see e.g. Refs. [23, 24]. In this sense, the present work can be considered as complementary to the studies based on two-dimensional billiard

systems. We have demonstrated that a tight connection between classical and quantum measures of chaos, embodied in the well-known Bohigas' conjecture [12], remains valid even under the condition of a strong energy dependence.

Another important conclusion of the work is the observed independence of quantum chaotic measures on the method used to quantize the system. Since the definition of quantum chaos is based on the system's semiclassical limit, it would be very surprising to find the opposite—i.e. statistical properties of spectra depending on the quantization. However, the question deserves to be further tested. The present work is probably only a first step in this direction.

Our results show that the Brody parameter, despite of being often deprecated, represents a reasonably sensitive measure of chaos in quantum system. This method enabled us to study the breakdown and reoccurrence of ordered quantal spectra with running parameter B in a much more detailed way.

Finally we have revitalized an almost 35 years old method by Peres [13] and showed its great potential in the field of quantum chaos and even beyond. Peres lattices provide an excellent viewpoint to the landscape around the border between classical and quantum physics. This is so especially for systems with two degrees of freedom whose lattices can be drawn as two-dimensional diagrams, in analogy with planar Poincaré sections of such systems. If applied within the domain of quantum chaos, Peres' method enables one to distinguish regular and chaotic behaviors on the level of individual states or subsets of states within the same energy interval. The structural information on individual eigenstates is represented by a single variable (the average of a suitably chosen observable), which allows one to use a simple visualization technique incorporating simultaneously a large number of states.

We showed that we can construct for one system more lattices with different Peres operators and that some of them are more suitable than others to capture the most essential dynamical features. The optimal choice of the Peres operator should be subject to further study. Although the Peres' method does not directly yield a calculable measure of quantum chaos, it represents an important indicator providing new insights into the origin of chaotic behavior.

The work summarizes our long-term effort to map chaotic properties of the geometric collective model of nuclear physics.. A great advantage of the geometric model (and also of the related interacting boson model) is the apparent conceptual simplicity encoding strikingly rich complexity of dynamics. Let us note that the above simplified models capture the main phenomenological features of nuclear collectivity which are presently beside a fully microscopic description. The study of disordered collective dynamics within these models may be considered as an attack to the problem of chaos in many-body systems from the direction perpendicular to the mean-field approach.

References

[1] A. Bohr, B. Mottelson, *Nuclear Structure*, Vol. II (World Scientific, Singapore, 1998).

[2] J. M. Eisenberg, W. Greiner, *Nuclear theory*, Vol. 1, *Nuclear Models* (North-Holland, Amsterdam, 1987).

[3] F. Iachello, A. Arima, *The Interacting Boson Model* (Cambridge University Press, Cambridge, United Kingdom, 1987).

[4] H. J. Stöckmann, *Quantum Chaos. An Introduction* (Cambridge University Press, Cambridge, UK, 1999).

[5] *Statistical Theories of Spectra: Fluctuations*, ed. C.E. Porter (Academic Press, New York, 1965).

[6] T. von Egidy, A.N. Behkami, H.H. Schmidt, "Nuclear level densities and level spacing distributions from 20F to 244Am", *Nuclear Physics A* **454**, 109 (1986); T. von Egidy, H.H. Schmidt, A.N. Behkami, "Nuclear level densities and level spacing distributions: Part II", *Nuclear Physics A* **481**, 189 (1988).

[7] O. Bohigas, P. Leboeuf, "Nuclear Masses: Evidence of Order-Chaos Coexistence", *Physical Review Letters* **88**, 092502 (2002).

[8] J.G. Hirsch, V. Velázquez, A. Frank, "Quantum chaos and nuclear mass systematics", *Physics Letters B* **595**, 231 (2004).

[9] Y. Alhassid, N. Whelan, "Chaotic properties of the interacting-boson model: A discovery of a new regular region", *Physical Review Letters* **67**, 816 (1991).

[10] N. Whelan, Y. Alhassid, "Chaotic properties of the interacting boson model", *Nuclear Physics A* **556**,, 42 (1993).

[11] V. Paar, D. Vorkapić, "Abul-Magd-Weidenmüller chaoticity effect: Evidence for interacting boson model?", *Physics Letters B* **205**, 7 (1988); "Quantum chaos for exact and broken K quantum number in the interacting-boson model", *Physical Review C* **41**, 2397 (1990); V. Paar, D. Vorkapić, A. E. L. Dieperink, "GOE-type energy level statistics and regular classical dynamics for rotational nuclei in the interacting boson model", *Physical Review Letters* **69**, 2184 (1992).

[12] O. Bohigas, M. J. Giannoni, C. Schmit, "Characterization of Chaotic Quantum Spectra and Universality of Level Fluctuation Laws", *Physical Review Letters* **52**, 1 (1984).

[13] A. Peres, "New Conserved Quantities and Test for Regular Spectra", *Physical Review Letters* **53**, 1711 (1984).

[14] G. Gneuss, U. Mosel, W. Greiner, "New Treatment of the Collective Nuclear Hamiltonian", *Physics Letters* **30B**, 161 (1969); "On The Relationship Between the Level-Structures in Spherical and Deformed Nuclei", *Physics Letters* **31B**, 269 (1970); "Even-Odd-Staggering in γ-Bands", *Physics Letters* **32B**, 161 (1970).

[15] Ch. Skokos, "Alignment indices: a new, simple method for determining the ordered or chaotic nature of orbits", *Journal of Physics A* **34**, 10029 (2001); Ch Skokos, Ch. Antonopoulos, T. C. Bountis, M. N. Vrahatis, "Detecting order and chaos in Hamiltonian systems by the SALI method", *Journal of Physics A* **37**, 6269 (2004).

[16] T. A. Brody, "Statistical measure for repulsion of energy-levels", *Lettere Nuovo Cimento* **7**, 482 (1973).

[17] M. C. Gutzwiller, *Chaos in Classical and Quantum Mechanics* (Springer-Verlag, New York, 1990).

[18] E. Chacón, M. Moshinsky, "Group theory of the collective model of the nucleus", *Journal of Mathematical Physics* **18**, 870 (1977).

[19] L. Horwitz, Y. B. Zion, M. Lewkowicz, M. Schiffer, J. Levitan, "Geometry of Hamiltonian chaos", *Physical Review Letters* **98**, 234301 (2007).

[20] I. C. Percival, "Regular and irregular spectra", *Journal of Physics B* **6**, L229 (1973).

[21] A. Csordás, R. Graham, P. Szépfalusy, G. Vattay, "Transition from Poissonian to Gaussian-orthogonal-ensemble level statistics in a modified Artin's billiard", *Physical Review E* **49**, 325 (1994).

[22] W. Li, L. E. Reichl, B. Wu, "Quantum chaos in a ripple billiard", *Physical Review E* **65**, 056220 (2002).

[23] M. Hénon, C. Heiles, "The Applicability of the Third Integral of Motion: Some Numerical Experiments", *Astronomical Journal* **69**, 73 (1964).

[24] E. Haller, H. Köppel, L. S. Cederbaum, "Uncovering the Transition from Regularity to Irregularity in a Quantum System", *Physical Review Letters* **52**, 1665 (1984).

List of original work

[**I**] P. Cejnar, P. Stránský
Regular and chaotic vibrations of deformed nuclei with increasing γ-rigidity
Physical Review Letters **93**, 102502 (2004)

[**II**] P. Stránský, M. Kurian, P. Cejnar
Classical chaos in the geometric collective model
Physical Review C **74**, 014306 (2006)

[**III**] M. Macek, P. Stránský, P. Cejnar, S. Heinze, J. Jolie, J. Dobeš
Classical and quantum properties of the semiregular arc inside the Casten triangle
Physical Review C **75**, 064318 (2007)

[**IV**] M. Macek, P. Stránský, P. Cejnar
Order and chaos in the interacting boson model
Physics of Atomic Nuclei **70**, sv. 9, 1592 (2007)

[**V**] P. Stránský, P. Cejnar, M. Macek
Order and chaos in the geometric collective model
Physics of Atomic Nuclei **70**, sv. 9, 1572 (2007)

[**VI**] P. Cejnar, P. Stránský
Impact of quantum phase transitions on excited level dynamics
Physical Review E **78**, 031130 (2008)
arXiv:0807.3649 [quant-ph]

[**VII**] P. Stránský, P. Hruška, P. Cejnar
Quantum chaos in the nuclear collective model: Classical-quantum correspondence
Physical Review E **79**, 046202 (2009)
arXiv:0902.3983 [quant-ph]

[**VIII**] P. Stránský, P. Hruška, P. Cejnar
Quantum chaos in the nuclear collective model: Peres Lattices
Physical Review E, in press
arXiv:0902.4155v1 [quant-ph]

[**IX**] P. Cejnar, P. Stránský, M. Macek
Quantum phase transitions and nuclear structure
International Journal of Modern Physics E, in press

[**X**] M. Macek, P. Stránský, P. Cejnar
Peres lattices in nuclear structure
International Journal of Modern Physics E, in press
arXiv:0810.2949 [nucl-th]

[**XI**] P. Cejnar, M. Macek, P. Stránský, M. Kurian
Regular and chaotic nuclear vibrations
in: Capture Gamma-Ray Spectroscopy and Related Topics, ed. A. Woehr, A. Aprahamian (AIP Conference Proceedings 819, 2006), p. 487

[**XII**] P. Cejnar, P. Stránský
Quantum phase transitions for excited states
in: Capture Gamma-Ray Spectroscopy and Related Topics, ed. A. Blazhev, J. Jolie, N. Warr, A. Zilges (AIP Conference Proceedings 1090, 2009), p. 169

[**XIII**] P. Stránský, M. Macek, P. Cejnar, J. Dobeš
Peres lattices in nuclear structure and beyond
in: Capture Gamma-Ray Spectroscopy and Related Topics, ed. A. Blazhev, J. Jolie, N. Warr, A. Zilges (AIP Conference Proceedings 1090, 2009), p. 174

[**XIV**] Interactive web presenting the main results
`http://www-ucjf.troja.mff.cuni.cz/~stransky/results`

Comment:

List of original work is sorted chronologically by the date of publication. The articles published in journals are written in black font, other works in gray font.